Estimating nonlinear interdependences in dynamical systems using cellular nonlinear networks

Dieter Krug,[1,2,*] Hannes Osterhage,[1,2] Christian E. Elger,[1] and Klaus Lehnertz[1,2,3,†]
[1]*Department of Epileptology, University of Bonn, Sigmund-Freud-Strasse 25, 53105 Bonn, Germany*
[2]*Helmholtz-Institute for Radiation and Nuclear Physics, University of Bonn, Nussallee 14-16, 53115 Bonn, Germany*
[3]*Interdisciplinary Center for Complex Systems, University of Bonn, Römerstrasse 164, 53117 Bonn, Germany*
(Received 11 July 2007; published 25 October 2007)

We propose a method for estimating nonlinear interdependences between time series using cellular nonlinear networks. Our approach is based on the nonlinear dynamics of interacting nonlinear elements. We apply it to time series of coupled nonlinear model systems and to electroencephalographic time series from an epilepsy patient, and we show that an accurate approximation of symmetric and asymmetric realizations of a nonlinear interdependence measure can be achieved, thus allowing one to detect the strength and direction of couplings.

DOI: 10.1103/PhysRevE.76.041916 PACS number(s): 87.19.La, 05.10.−a, 05.45.Tp, 07.05.Mh

I. INTRODUCTION

Synchronization phenomena play an important role in nearly all fields of science, including physics, chemistry, economy, biology, and neurosciences (see Refs. [1,2] for an overview). The human brain can be regarded as a prominent example in which different forms of synchronization can be observed. From neurophysiology it is known that interactions between specific regions of the brain are responsible to ensure the normal functioning of the brain [3]. A substantial change in these interactions may give rise to certain malfunctions of the brain such as Parkinson's disease or ataxia. A malfunction of the brain that is known to be particularly associated with a pathological increase in synchronization is the disease epilepsy along with its cardinal symptom, the epileptic seizure. Led by a growing interest in the possibility of seizure prediction, research over the last years has shown that the analysis of synchronization phenomena in the epileptic brain can contribute significantly to this field (see Ref. [4] for an overview). In contrast to previously used—mostly linear and nonlinear univariate—time-series analysis approaches, a significant predictive performance above chance level can be achieved for different measures of synchronization [5–8]. This interest has also been facilitated by the fact that measurements of the electrical activity of brain neural networks are readily available in the form of the electroencephalogram (EEG) measured by electrodes placed on the surface of or even within the skull. In current clinical or neuroscientific settings the number of sensoring electrodes typically ranges between 100 and 200. Bivariate analyses of synchronization phenomena require computational resources that grow quadratically with the number of channels, which limits real-time applications to a certain extent.

Artificial neural networks (ANNs) are computational tools that have found extensive utilization in solving complex real-world problems. The attractiveness of ANNs comes from their information-processing characteristics such as intrinsic nonlinearity, high parallelism, and fault and noise tolerance. More importantly, neural networks are able to learn a rule from a set of examples [9] and, after successful supervised or unsupervised learning, are capable of generalization. ANNs have already been successfully applied to model, to generate, or to predict time series, including chaotic ones [10–20]. Nevertheless, since a conventional (i.e., von Neumann) computer architecture is not well suited to simulate large-scale neural networks, there is the need for a special parallel architecture that even allows mobile field applications. Cellular nonlinear networks (CNNs) [21,22] combine the architecture of cellular automata and neural networks. A CNN is an array of locally coupled nonlinear electrical circuits or cells, which is capable of processing a large amount of information in parallel and in real time. Interactions between the cells of a CNN are only local and usually translation invariant; i.e., a connection from a cell j toward another cell i only exists if j is part of i's neighborhood $\mathcal{U}(i)$ and its type and strength depend only on the relative position of j with respect to i. Thus the number of connections increases only linearly with the number of cells, a property that already enabled hardware realization of CNNs [e.g., very-large-scale integrated implementations (VLSIs) [23–25]], as opposed to other types of ANNs. Recent studies showed that a sufficient estimation of characterizing measures [26–29], including measures for phase synchronization [30], can be achieved using CNNs.

We here show that the approach of analyzing the dynamics of interacting complex systems with the nonlinear dynamics of interacting nonlinear elements can also be extended to the concept of generalized synchronization [31–34]. Among the many time-series analysis techniques that have been proposed to measure generalized synchronization [33–36], estimates for nonlinear interdependences [37,38] turned out to be the most reliable way of assessing the extent of generalized synchronization in field applications [38–42]. With this approach the existence of a functional relation between two systems is not assumed and interdependences are quantified by evaluating how neighborhoods (i.e., recurrences) in one reconstructed state space map into the other. Measures for nonlinear interdependence are generally asymmetric which, in principle, provide a means to detect *driver-responder* relationships by identifying the *more active* system.

This article is organized as follows. In Sec. II A we briefly recall the definitions for the nonlinear interdependence mea-

*krug@uni-bonn.de
†klaus.lehnertz@ukb.uni-bonn.de

sure N. The methods used to approximate N with a cellular nonlinear network are presented in Sec. II B. In Sec. III we show the results of our application to time series from model systems and to multiday EEG time series from an epilepsy patient, before we draw our conclusions in Sec. IV.

II. METHODS

A. Measuring nonlinear interdependence

Following Refs. [37,38] the nonlinear interdependence N is defined as follows. Given two dynamical systems V and W, let $\mathbf{v}_n=(v_n,\ldots,v_{n-(m-1)d})$ and $\mathbf{w}_n=(w_n,\ldots,w_{n-(m-1)d})$, $n=1,\ldots,K$, denote their reconstructed delay vectors in state space [43], where m denotes the embedding dimension and d the time delay. Let $r_{n,j}$ and $s_{n,j}, j=1,\ldots,k$, denote the time indices of the k nearest neighbors of $\mathbf{v}_n$ and $\mathbf{w}_n$, respectively. For each $\mathbf{v}_n$, the mean-squared Euclidean distance to its k neighbors is denoted by

$$R_n^{(k)}(V)=\frac{1}{k}\sum_{j=1}^{k}(\mathbf{v}_n-\mathbf{v}_{r_{n,j}})^2. \tag{1}$$

In addition, the *W-conditioned* mean-squared Euclidean distance is derived by replacing the nearest neighbors by the equal-time partners of the closest neighbors of $\mathbf{w}_n$:

$$R_n^{(k)}(V|W)=\frac{1}{k}\sum_{j=1}^{k}(\mathbf{v}_n-\mathbf{v}_{s_{n,j}})^2. \tag{2}$$

The nonlinear interdependence measure N is defined as

$$N^{(k)}(V|W)=\frac{1}{K}\sum_{n=1}^{K}\frac{R_n(V)-R_n^{(k)}(V|W)}{R_n(V)}, \tag{3}$$

where

$$R_n(V)=\frac{1}{K-1}\sum_{j\neq n}(\mathbf{v}_n-\mathbf{v}_j)^2 \tag{4}$$

denotes the mean distance of $\mathbf{v}_n$ to all other vectors in state space. Low values of $N^{(k)}(V|W)$ indicate independence between systems V and W (note that slightly negative values are possible), whereas $N^{(k)}(V|W)\to 1$ for identical systems. The opposite interdependence $N^{(k)}(W|V)$ is defined in complete analogy. As $N^{(k)}(W|V)$ in general is not equal to $N^{(k)}(V|W)$, this asymmetry can be exploited to obtain information about driver-responder relationships. We here quantify the degree of generalized synchronization by

$$N_s^{(k)}=\frac{N^{(k)}(V|W)+N^{(k)}(W|V)}{2} \tag{5}$$

and the asymmetry by

$$N_a^{(k)}=\frac{N^{(k)}(V|W)-N^{(k)}(W|V)}{2}. \tag{6}$$

For the latter positive (negative) values can indicate driver-responder relationships [with V being the driver (responder) and W being the responder (driver)] and thus can yield information about directionality of coupling between V and W in a sense that one system can be interpreted as more active than the other. If not stated otherwise, we used $k=6$ nearest neighbors [44,45] in our simulations and substitute $N_s^{(6)}$ by N_s and $N_a^{(6)}$ by N_a.

B. Estimating nonlinear interdependence with cellular nonlinear networks

Since the general concepts for a CNN-based estimation of a (univariate or bivariate) characterizing measure have been described in detail in Refs. [28–30], we here give only a brief account on the applied methodological steps. We consider a CNN which consists of a two-dimensional $M_x\times M_y$ homogeneous lattice of cells with local nonlinear interactions. The corresponding state equation for cell (i,j) reads

$$\frac{d}{d\tau}\kappa_{i,j}(\tau)=-\kappa_{i,j}(\tau)+\sum_{k,l\in\mathcal{U}_A}A_{k,l}(\mu_{i-k,j-l}(\tau))+\sum_{k,l\in\mathcal{U}_B}B_{k,l}(\eta_{i-k,j-l})+Z, \tag{7}$$

where $\kappa_{i,j}(\tau)$ denotes the state variable of cell (i,j) and $\mu_{k,l}(\tau)$ the output variable of cell (k,l) according to

$$\mu_{k,l}(\tau)=f(\kappa_{k,l}(\tau))=\frac{2}{1+e^{-4\kappa_{k,l}(\tau)}}-1, \tag{8}$$

given an external input variable $\eta_{k,l}$ as well as feedback and feed-forward template functions $A_{k,l}$ and $B_{k,l}$ (with spheres of influence $k,l\in\mathcal{U}_A$ or $\in\mathcal{U}_B$), respectively. Z denotes a global cell bias. The template function A operates on the outputs of cell (k,l) and the template function B operates on the external inputs in the neighborhood of cell (k,l). Both templates and the cell bias Z have to be determined (e.g., by some learning algorithm) to achieve the desired CNN behavior. In order to determine an appropriate CNN with cell outputs showing the behavior of the nonlinear interdependences N_s and N_a, we performed all simulations using a full feature simulation system (cf. Ref. [46]). We restricted ourselves to a quadratic network arrangement ($M_x=M_y$) with a minimum possible 3×3 neighborhood size as well as to polynomial-type template functions

$$A_{k,l}^{(P)}(\mu)=\sum_{p=1}^{P}a_{k,l}^{(p)}\mu^p,$$

$$B_{k,l}^{(Q)}(\eta)=\sum_{q=1}^{Q}b_{k,l}^{(q)}\eta^q, \tag{9}$$

of order $P=Q=3$. We used the so-called *closed spiral* boundary condition where all boundary cells are connected to the other side of the network, but the connection has an offset of 1 for each row. In order to present the time series to the network, we used a line wise alignment (i.e., the rightmost cell in a row is connected to the leftmost cell in the following row) of the time series, where time series v_n, $n=1,\ldots,J$, was assigned to the input η and w_n to the initial state $\kappa(0)$ of the CNN [28–30]. Together with the chosen boundary condition

this alignment preserves the temporal order of the time series. Following Ref. [46] simulations were performed not up to a steady state [i.e., $\mu(\tau)\rightarrow\mu(\infty)$], but up to some fixed transient time τ_{trans}. For this purpose we integrated Eq. (7) using Euler's method with a step size of $h=0.2$ and 100 integration steps resulting in a transient time $\tau_{trans}=20$.

In order to train the network we randomly selected L representative pairs of time series (see Sec. III) along with their corresponding values of the nonlinear interdependences N_s (and N_a) (see Sec. II A). Half of these values were taken from the interval $[N_s^{\text{low}}-\rho^{\text{low}},N_s^{\text{low}}+\rho^{\text{low}}]$ representing weakly dependent time series. The other half was from the interval $[N_s^{\text{high}}-\rho^{\text{high}},N_s^{\text{high}}+\rho^{\text{high}}]$ representing stronger dependent time series. ρ^{low} and ρ^{high} adjust the size of the intervals such that N_s values from at least $\frac{L}{2}$ time series are confined to these intervals. The desired output μ^{Ref} was set to +1 for N_s^{high} and to −1 for N_s^{low}. Selections and assignments for N_a are defined in complete analogy. N_a^{low} indicates no asymmetry and $|N_a^{\text{high}}|$ indicates a driver-responder relationship.

After choosing random initial values for the components of templates A and B and for the global cell bias Z the following cost function was minimized iteratively using an evolutionary optimization algorithm (population size 50; survivors 10; immigrants per generation 10; iteration steps 30 000) [47–49] and our distributed computing system [50]:

$$\Gamma=\frac{1}{L}\sum_{l=0}^{L-1}\left(\frac{1}{4M_xM_y}\sum_{m=0}^{M_xM_y-1}(\mu_{m,l}(\tau_{\text{trans}})-\mu_l^{\text{Ref}})^2\right). \quad (10)$$

The approximated nonlinear interdependence N_s^{CNN} is defined as

$$N_s^{\text{CNN}}=\left(\frac{N_s^{\text{high}}-N_s^{\text{low}}}{M_xM_y}\sum_{m=0}^{M_xM_y-1}\frac{\mu_m(\tau_{\text{trans}})+1}{2}\right)+N_s^{\text{low}}. \quad (11)$$

N_a^{CNN} is defined in complete analogy.

III. APPLICATIONS

We start by applying our CNN-based approach to approximate nonlinear interdependences from time series of exemplary model systems in order to test our method on well-known experimental setups. For the basic CNN structure we restricted ourselves to parameters specified by already available CNN hardware realizations [51,52]. We studied coupled systems with similar dynamics as well as coupled structurally different dynamical systems, which allowed us to simulate the different situations which might occur when analyzing field data. We employed unidirectional or bidirectional diffusive couplings and varied the coupling strength ϵ such as to cover the range from *no synchronization* to *full synchronization*. For each coupling strength we generated 20 realizations (taking randomly chosen points in the state spaces near the systems' attractors as initial conditions for the differential equations) and calculated N_s and N_a according to Eqs. (5) and (6). We linearly mapped the amplitude range of the normalized (zero mean) time series to the CNN range of $[-1,1]$. For each setup we then compiled a training set consisting of $L=10$ pairs of time series along with their corresponding values of the nonlinear interdependences (see Sec. II B), which we used for an in-sample optimization of our CNN. With the remaining $L_w=20n_\epsilon-L$ pairs of time series we performed an out-of-sample validation of our approach, quantifying the goodness of our CNN-based approximation of strength and direction of interdependence by

$$\delta_s=\frac{1}{L_w}\sum_{i=0}^{L_w-1}|N_s^{\text{CNN}}(i)-N_s(i)|,$$

$$\delta_a=\frac{1}{L_w}\sum_{i=0}^{L_w-1}|N_a^{\text{CNN}}(i)-N_a(i)|, \quad (12)$$

and by calculating the Spearman rank-order correlation coefficient ρ between the $N_{s,a}^{\text{CNN}}$ and $N_{s,a}$ values from the respective realizations.

A. Model systems with similar dynamics

Our first example is given by coupled Rössler dynamics:

$$\dot{x}_1=-\omega_1y_1-z_1+\epsilon_{21}(x_2-x_1),$$

$$\dot{y}_1=\omega_1x_1+0.165y_1,$$

$$\dot{z}_1=0.2+z_1(x_1-10),$$

$$\dot{x}_2=-\omega_2y_2-z_2+\epsilon_{12}(x_1-x_2),$$

$$\dot{y}_2=\omega_2x_2+0.165y_2,$$

$$\dot{z}_2=0.2+z_2(x_2-10), \quad (13)$$

with a slight mismatch of the natural frequencies $\omega_1=0.89$ and $\omega_2=0.85$. Equations (13) were integrated using a standard fourth-order Runge-Kutta routine with a step size of 0.1. In order to eliminate transients the first 10^3 iterations were discarded.

For evaluating the symmetric nonlinear interdependence N_s we increased the coupling strength $\epsilon=\epsilon_{12}=\epsilon_{21}$ (bidirectional coupling) between $0\leq\epsilon\leq0.04$ in $n_\epsilon=41$ steps ($\Delta\epsilon=0.001$) and generated time series of the x components of the systems consisting of $J=4096$ data points each. For each coupling strength we calculated N_s using an embedding dimension of $m=7$ [53] and a time delay of $d=14$, which approximately corresponds to the decorrelation times of the systems [54]. Given the number of data points we used a CNN with $M_x=M_y=64$ cells [51] and assigned the x component of the first system to the CNN input η and the x component of the second system to the initial state $\kappa(0)$ [cf. Eq. (7)]. For the in-sample optimization of the CNN we compiled a training set, which consisted of $L=10$ randomly selected pairs of time series along with their respective N_s values taken from the intervals defined by $N_s^{\text{low}}=0$ with $\rho^{\text{low}}=0.08$ and by $N_s^{\text{high}}=0.9$ with $\rho^{\text{high}}=0.07$. We obtained $\Gamma=3.374\times10^{-3}$.

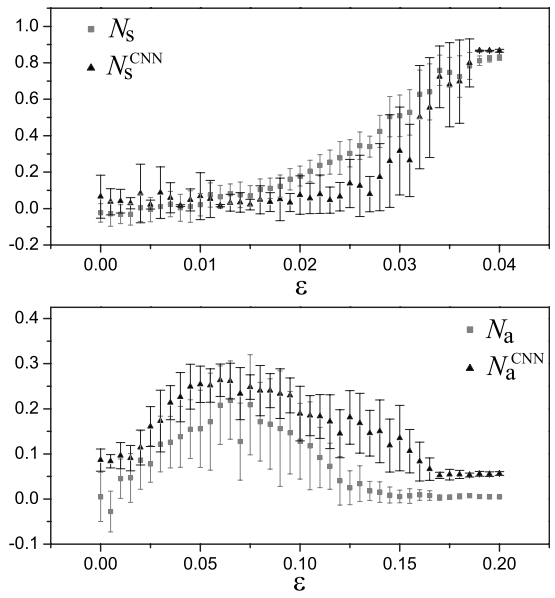

FIG. 1. Top: means and standard deviations of the calculated (N_s) and approximated (N_s^{CNN}) symmetric nonlinear interdependence for coupled Rössler systems using different coupling strength ϵ. Bottom: same as above but for the asymmetric nonlinear interdependence (N_a and N_a^{CNN}).

The results of an out-of-sample validation are shown in Fig. 1 (upper panel) where we plot the dependence of N_s and of N_s^{CNN} on the coupling strength ϵ. These findings indicate that our CNN allows one to approximate the symmetric nonlinear interdependence N_s with a sufficient accuracy ($\delta_s=0.13$, $\rho=0.66$, $p<0.001$). We observed a slightly delayed increase of N_s^{CNN} in the range $0.02<\epsilon<0.03$. The larger variance of N_s^{CNN} may reflect the cells' tendency toward maximum (N_s^{high}) or minimum values (N_s^{low}) due to the sigmoidal output function [cf. Eq. (8)].

For evaluating the asymmetric nonlinear interdependence N_a we set $\epsilon_{21}=0$ (unidirectional coupling with system 1 being the driver) and increased the coupling strength $\epsilon=\epsilon_{12}$ between $0\leq\epsilon\leq0.2$ in $n_\epsilon=41$ steps ($\Delta\epsilon=0.005$). For each coupling strength we calculated N_a using embedding parameters as before. We proceeded as described above but compiled another training set that consisted of $L=10$ randomly selected pairs of time series along with their respective N_a values taken from the intervals defined by $N_a^{low}=-0.05$ with $\rho^{low}=0.05$ and by $N_a^{high}=0.33$ with $\rho^{high}=0.02$. We obtained $\Gamma=0.082$ for the in-sample optimization.

The results of an out-of-sample validation are shown in the lower panel of Fig. 1 and indicate that, overall, our CNN also allows one to approximate the asymmetric nonlinear interdependence N_a with a sufficient accuracy ($\delta_a=0.09$, $\rho=0.74$, $p<0.001$). Particularly in the range of weak couplings ($0.025<\epsilon<0.15$) N_a^{CNN} allows one to identify the driving system.

B. Structurally different dynamical model systems

Our second example is given by unidirectionally coupled Rössler (driver) and Lorenz (responder) dynamics:

$$\dot{x}_1 = -0.89y_1 - z_1,$$

$$\dot{y}_1 = 0.89x_1 + 0.165y_1,$$

$$\dot{z}_1 = 0.2 + z_1(x_1 - 10),$$

$$\dot{x}_2 = -\frac{8}{3}x_1 + y_1z_1 + \epsilon(x_1 - x_2),$$

$$\dot{y}_2 = 28z_2 - y_2 - x_2z_2,$$

$$\dot{z}_2 = 10(y_2 - z_2). \tag{14}$$

The equations of motion were integrated using a standard fourth-order Runge-Kutta routine with a step size of 0.01. In order to eliminate transients the first 10^4 iterations were discarded. We increased the coupling strength between $0.6\leq\epsilon\leq2.4$ in $n_\epsilon=45$ steps ($\Delta\epsilon=0.04$) and generated time series of the systems consisting of $J=16\,384$ data points each. For each coupling strength we calculated N_s and N_a using an embedding dimension of $m=5$ [44] and, given the different characteristic recurrence times of the systems, a minimum possible time delay $d=1$. Given the number of data points we used a CNN with $M_x=M_y=128$ cells [52] and assigned the x component of the driver to the CNN input η and the y component of the responder to the initial state $\kappa(0)$ [cf. Eq. (7)].

For evaluating the symmetric nonlinear interdependence N_s we compiled a training set of $L=10$ randomly selected pairs of time series along with their respective N_s values taken from the intervals defined by $N_s^{low}=0$ with $\rho^{low}=0.02$ and by $N_s^{high}=0.65$ with $\rho^{high}=0.02$. For the in-sample optimization we obtained $\Gamma\approx0$, indicating a perfect performance for this training set. The out-of-sample validation (see upper panel of Fig. 2) shows that our CNN allows one to approximate the dependence of N_s on ϵ also for structurally different systems with a sufficient accuracy ($\delta_s=0.11$, $\rho=0.75$, $p<0.001$).

For the asymmetric nonlinear interdependence N_a we compiled a training set of $L=10$ randomly selected pairs of time series along with their respective N_a values taken from the intervals defined by $N_a^{low}=-0.1$ with $\rho^{low}=0.01$ and by $N_a^{high}=0.35$ with $\rho^{high}=0.15$. For the in-sample optimization we obtained $\Gamma=0.137$, but the out-of-sample validation ($\delta_a=0.046$, $\rho=0.36$, $p<0.001$) indicated a sufficient approximation (as shown in the lower panel of Fig. 2). Interestingly, for uncoupled systems and when the systems begin to synchronize we now obtained an almost perfect approximation of N_a. Again in the range of weak couplings ($0.8<\epsilon<1.1$), N_a^{CNN} allows one to identify the driving system.

Summarizing this section, we conclude that our CNN allows one to approximate both symmetric and asymmetric nonlinear interdependences with a sufficient accuracy. Taking into account the rather limited range of both N_s and N_a values used for optimizing the CNN and the small number of data points the time series consisted of, we regard the achieved approximation accuracy as sufficiently good, particularly for field applications. Such an application that aims

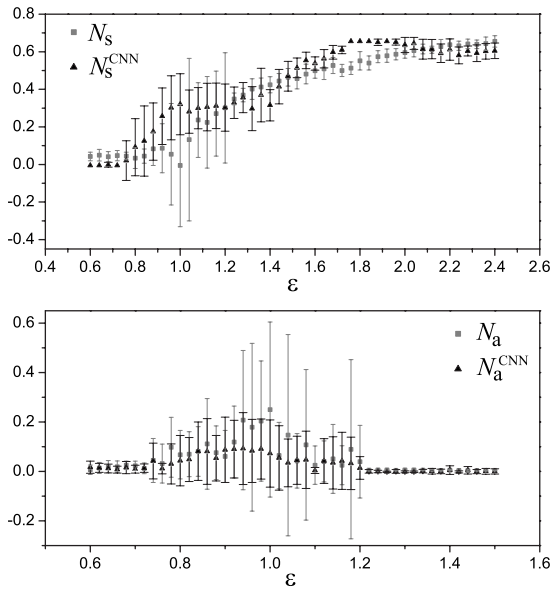

FIG. 2. Top: means and standard deviations of the calculated (N_s) and approximated (N_s^{CNN}) symmetric nonlinear interdependence for coupled Rössler (driver) and Lorenz (responder) systems using different coupling strengths ϵ. Bottom: same as above but for the asymmetric nonlinear interdependence (N_a and N_a^{CNN}).

at differentiating between strong and only weak interactions will be presented in the next subsection.

C. EEG data

We analyzed a multichannel EEG that was recorded for a period of 5 days from an epilepsy patient. The patient had signed informed consent that the clinical data might be used and published for research purposes. The study protocol had previously been approved by the ethics committee of the University of Bonn. The patient had ten epileptic seizures of focal origin occurring spontaneously within the second half of the recording period. The EEG was measured from electrodes implanted directly within the brain prior to and independently from the design of this study during the presurgical work-up. EEG data were sampled at 200 Hz using a 16-bit analog-to-digital converter and filtered within a frequency band of 0.5–85 Hz. We here restrict ourselves to the analysis of EEG data from two sets (P_1, P_2) of pairs of recording channels. Previous studies [5,30] have shown that the temporal evolution of measures characterizing the strength of synchronization (including N_s) calculated for set P_1 exhibited highest seizure prediction performance. We here repeated the analyses presented in Ref. [5] for the asymmetric nonlinear interdependence N_a and assigned to set P_2 the pair of recording channels for which N_a exhibited highest seizure prediction performance. We note that the identified channels in sets P_1 and P_2 are not identical but are confined to the same brain region (medial temporal lobe).

Due to the high amplitude variability of the EEG, we linearly mapped, as an additional preprocessing step, the amplitude range of $[-150,150]$ mV of the normalized (zero mean) EEG to the CNN range of $[-1,1]$. N_s and N_a values were then calculated (see Sec. II A) using a moving-window technique with nonoverlapping segments of 20.48 s corresponding to $J=4096$ data points. We followed Ref. [37] and used an embedding dimension of $m=10$, a time delay of $d=25$, and $k=10$ nearest neighbors. The number of $N_s^{(10)}$ and $N_a^{(10)}$ values for each set amounted to 18 735.

We compiled two training sets (one for P_1 and one for P_2) by randomly selecting $L=16$ EEG segments along with their corresponding $N_s^{(10)}$ and $N_a^{(10)}$ values using criteria defined in Sec. II B, but without knowledge of the actual patient's state (awake, asleep, seizure activity, pre- or post-seizure activity, etc.). For evaluating the symmetric nonlinear interdependence we used $N_s^{(10)}$ values from the intervals defined by $N_s^{\text{low}}=0.3$ with $\rho^{\text{low}}=0.01$ and by $N_s^{\text{high}}=0.85$ with $\rho^{\text{high}}=0.01$ and obtained $\Gamma=0.017$ for the in-sample optimization. For the asymmetric nonlinear interdependence we used $N_a^{(10)}$ values from the intervals defined by $N_a^{\text{low}}=-0.14$ with $\rho^{\text{low}}=0.04$ and by $N_a^{\text{high}}=0.15$ with $\rho^{\text{high}}=0.03$. The in-sample optimization yielded $\Gamma=0.102$.

The obtained CNN settings for P_1 and P_2 were then used to calculate N_s^{CNN} and N_a^{CNN} for the *test sets*, which consisted of the remaining 18 719 time series pairs. For the symmetric nonlinear interdependence we observed that the CNN produced N_s^{CNN} that were constantly lower than the corresponding $N_s^{(10)}$ values but the overall temporal variability is reproduced with a sufficient quality. We therefore performed an offset correction by adding a constant value $\vartheta=\langle N_s^{(10)}\rangle_t - \langle N_s^{\text{CNN}}\rangle_t \cong 0.16$ ($\langle\cdot\rangle_t$ denotes the temporal average) to all N_s^{CNN} values before quantifying the goodness of our CNN-based approximation, which yielded $\delta_s=0.06$ ($\rho=0.79$; $p<0.001$). In Fig. 3 we present the temporal evolution of the calculated and the approximated symmetric nonlinear interdependences. For the asymmetric nonlinear interdependence no offset correction was necessary, and in Fig. 4 we present the temporal evolution for this measure. Here the out-of-sample validation yielded $\delta_a=0.033$ ($\rho=0.50$, $p<0.001$). Although both N_s^{CNN} and N_a^{CNN} exhibited a higher variance, the overall temporal variability of the nonlinear interdependence is reproduced with a sufficient quality, despite the extremely small subset of data used to train the network (a recording time of about 330 s only).

In order to assess the suitability of our CNN-based approach for a possible application in seizure prediction studies, we evaluated the success of predictions (in terms of sensitivity and specificity) via a receiver-operating characteristics (ROC) statistic [55,56]. Following Ref. [5] we assumed that for each of the ten seizures a preseizure state with a duration of 4 h exists. Using ROC, we compared the frequency distributions of the symmetric nonlinear interdependence values from the preseizure states and from the seizure-free interval (excluding data from the seizure states and from the 30 min following the seizures). Our CNN-based approach yielded a prediction performance of ROC=0.74, which was lower than for the calculated nonlinear interdependence (ROC=0.83). Given the observed higher variance of the CNN-based estimates, this deviation was to be expected to some extent. The achieved performance, however, can still be regarded as promising and indicates that a differ-

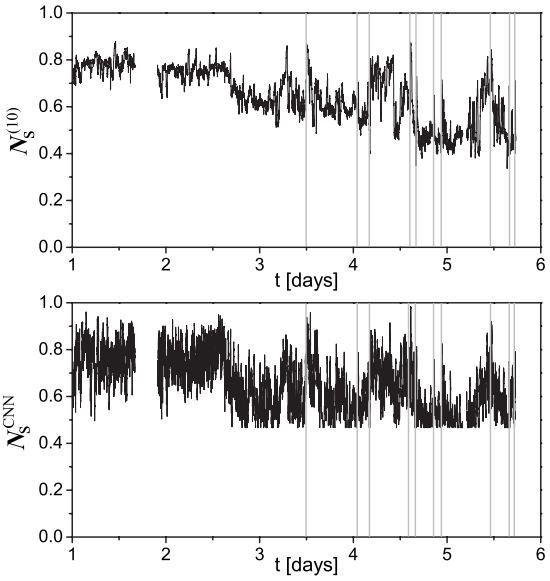

FIG. 3. Calculated (top) and offset-corrected approximated (bottom) symmetric nonlinear interdependence for set P_1. Seizure onsets are marked by gray vertical lines. Profiles are smoothed using a 14-point moving-average filter for better visualization. Twice the patient was briefly (13 and 54 min) disconnected from the EEG acquisition system. A longer discontinuity (340 min) was necessary to carry out a magnetic resonance imaging scan to determine the exact location of the implanted electrodes.

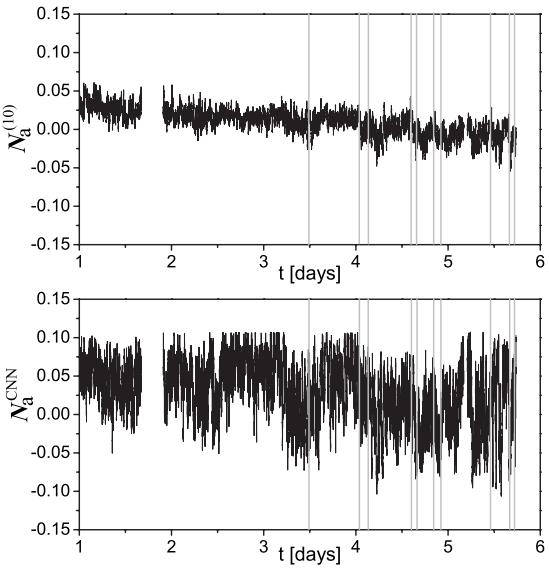

FIG. 4. Same as Fig. 3 but for the asymmetric nonlinear interdependence and for set P_2.

entiation of preseizure states from the seizure-free interval is in principle possible using our CNN-based approach.

IV. CONCLUSIONS

We have shown that cellular nonlinear networks are well suited to identify different aspects of generalized synchronization from a pair of measured time series. Both a symmetric and an asymmetric measure for nonlinear interdependence (N_s, N_a) could be approximated with a sufficient accuracy using the nonlinear dynamics of interacting nonlinear elements. Applying this concept to time series of coupled nonlinear model systems and to electroencephalographic time series from an epilepsy patient we have shown that strength and direction of couplings can be detected, which extends our previous findings on approximating a measure for phase synchronization with CNNs [30].

Our CNN-based estimates N_s^{CNN} and N_a^{CNN} exhibited a comparably larger statistical spread, in general. Nevertheless, using N_s^{CNN} it was possible to distinguish regimes of low coupling, weak synchronization, and full synchronization in time series from model systems with similar dynamics and from structurally different model systems. N_a^{CNN} allowed us to detect directional couplings. Applying our method to EEG time series, we could show our CNNs to be capable of reproducing long-term variations of the symmetric and the asymmetric part of the nonlinear interdependence in continuous, multiple-day EEG recordings from an epilepsy patient. Since this was possible even without using *a priori* knowledge as to the various states of the patients (e.g., awake, asleep, or seizure activity) when optimizing our CNN, we consider our approach as a possible basis for medical applications (e.g., a miniaturized analysis system for the prediction of seizures). We note though that our findings are, at present, restricted to simulated or digital realizations of CNNs. Nevertheless, polynomial-type hardware CNN's (VLSIs) are already available [57,58], and even nonlinear templates can well be approximated by piecewise linear functions [59]. Moreover, with on-chip optimization strategies [60] robust templates (derived from simulated or digital CNNs) can be obtained, thereby minimizing the effect of hardware tolerance.

ACKNOWLEDGMENTS

We would like to thank Ronald Tetzlaff and his group for close support. This work was supported by the Deutsche Forschungsgemeinschaft (Grant No. LE 660/2-3).

[1] A. S. Pikovsky, M. G. Rosenblum, and J. Kurths, *Synchronization—A universal concept in nonlinear sciences* (Cambridge University Press, Cambridge, UK, 2001).

[2] S. Boccaletti, J. Kurths, G. Osipov, D. L. Valladare, and C. S. Zhou, Phys. Rep. **366**, 1 (2002).

[3] L. Glass, Nature (London) **410**, 277 (2001).

[4] F. Mormann, R. G. Andrzejak, C. E. Elger, and K. Lehnertz, Brain **130**, 314 (2007).

[5] F. Mormann, T. Kreuz, C. Rieke, R. G. Andrzejak, A. Kraskov, P. David, C. E. Elger, and K. Lehnertz, Clin. Neurophysiol.

116, 569 (2005).
[6] M. Le Van Quyen, J. Soss, V. Navarro, R. Robertson, M. Chavez, M. Baulac, and J. Martinerie, Clin. Neurophysiol. **116**, 559 (2005).
[7] B. Schelter, M. Winterhalder, T. Maiwald, A. Brandt, A. Schad, A. Schulze-Bonhage, and J. Timmer, Chaos **16**, 013108 (2006).
[8] H. Osterhage, F. Mormann, M. Staniek, and K. Lehnertz, Int. J. Bifurcation Chaos Appl. Sci. Eng. (to be published).
[9] T. L. H. Watkin, A. Rau, and M. Biehl, Rev. Mod. Phys. **65**, 499 (1993).
[10] A. M. Albano, A. Passamante, T. Heidiger, and M. E. Farrell, Physica D **58**, 1 (1992).
[11] J. Principe, A. Rathie, and J. Kuo, Int. J. Bifurcation Chaos Appl. Sci. Eng. **2**, 989 (1992).
[12] E. Eisenstein, I. Kanter, D. A. Kessler, and W. Kinzel, Phys. Rev. Lett. **74**, 6 (1995).
[13] D. R. Kulkarni, J. C. Parikh, and R. Pratap, Phys. Rev. E **55**, 4508 (1997).
[14] R. Bakker, J. C. Schouten, C. L. Giles, F. Takens, and C. M. van den Bleek, Neural Comput. **12**, 2355 (2000).
[15] A. Freking, W. Kinzel, and I. Kanter, Phys. Rev. E **65**, 050903(R) (2002).
[16] M. Small and C. K. Tse, Phys. Rev. E **66**, 066701 (2002).
[17] S. H. Chun and S. H. Kim, Expert. Sys. **21**, 192 (2004).
[18] M. Ciszak, J. M. Gutierrez, A. S. Cofino, C. Mirasso, R. Toral, L. Pesquera, and S. Ortin, Phys. Rev. E **72**, 046218 (2005).
[19] N. G. Pavlidis, D. K. Tasoulis, V. P. Plagianakos, and M. N. Vrahatis, Int. J. Bifurcation Chaos Appl. Sci. Eng. **16**, 2053 (2006).
[20] R. Gareta, L. M. Romeo, and A. Gil, Energy Convers. Manage. **47**, 1770 (2006).
[21] L. O. Chua and L. Yang, IEEE Trans. Circuits Syst. **35**, 1257 (1988).
[22] L. O. Chua and L. Yang, IEEE Trans. Circuits Syst. **35**, 1273 (1988).
[23] S. Espejo, R. Carmona, R. Dominguez-Castro, and A. Rodriguez-Vazquez, Int. J. Circuit Theory Appl. **24**, 93 (1996).
[24] Z. Nagy and P. Szolgay, IEEE Trans. Circuits Syst., I: Fundam. Theory Appl. **50**, 774 (2003).
[25] J. J. Martinez, F. J. Toledo, and J. M. Ferrandez, Lect. Notes Comput. Sci. **2687**, 33 (2003).
[26] R. Tetzlaff, R. Kunz, C. Ames, and D. Wolf, in *Proceedings of the IEEE European Conference on Circuit Theory and Design*, edited by C. Beccari, M. Biey, P. Civalleri, and M. Gilli (Levrotto & Bella, Turin, Italy, 1999), pp. 1007–1010.
[27] A. Potapov and M. K. Ali, Phys. Rev. E **65**, 046212 (2002).
[28] R. Kunz and R. Tetzlaff, J. Circuits Syst. Comput. **12**, 825 (2003).
[29] R. Tetzlaff, T. Niederhofer, and P. Fischer, Int. J. Circuit Theory Appl. **34**, 89 (2006).
[30] R. Sowa, A. Chernihovskyi, F. Mormann, and K. Lehnertz, Phys. Rev. E **71**, 061926 (2005).
[31] H. Fujisaka and T. Yamada, Prog. Theor. Phys. **69**, 32 (1983).
[32] V. S. Afraimovich, N. N. Verichev, and M. I. Ravinovich, Izv. VUZ. Radiophiz. **29**, 795 (1986).
[33] N. F. Rulkov, M. M. Sushchik, L. S. Tsimring, and H. D. I. Abarbanel, Phys. Rev. E **51**, 980 (1995).
[34] H. D. I. Abarbanel, N. F. Rulkov, and M. M. Sushchik, Phys. Rev. E **53**, 4528 (1996).
[35] S. J. Schiff, P. So, T. Chang, R. E. Burke, and T. Sauer, Phys. Rev. E **54**, 6708 (1996).
[36] M. Le Van Quyen, J. Martinerie, C. Adam, and F. J. Varela, Physica D **127**, 250 (1999).
[37] J. Arnhold, P. Grassberger, K. Lehnertz, and C. E. Elger, Physica D **134**, 419 (1999).
[38] R. Quian Quiroga, A. Kraskov, T. Kreuz, and P. Grassberger, Phys. Rev. E **65**, 041903 (2002).
[39] J. Bhattacharya, H. Petsche, and E. Pereda, J. Neurosci. **21**, 6329 (2001).
[40] C. J. Stam and B. W. van Dijk, Physica D **163**, 236 (2002).
[41] R. G. Andrzejak, A. Ledberg, and G. Deco, New J. Phys. **8**, 6 (2006).
[42] H. Osterhage, F. Mormann, T. Wagner, and K. Lehnertz, Int. J. Neural Syst. **17**, 139 (2007).
[43] F. Takens, in *Dynamical Systems and Turbulence*, edited by D. A. Rand and L. S. Young, Vol. 898 of Lecture Notes in Mathematics (Springer-Verlag, Berlin, 1980), pp. 366–381.
[44] R. Quian Quiroga, J. Arnhold, and P. Grassberger, Phys. Rev. E **61**, 5142 (2000).
[45] D. A. Smirnov and R. G. Andrzejak, Phys. Rev. E **71**, 036207 (2005).
[46] R. Kunz, R. Tetzlaff, and D. Wolf, in *Proceedings of the IEEE International Symposium on Circuits and Systems*, edited by J. Vandevalle and M. Hassler (IEEE, Piscataway, NJ, 2000), pp. 1024–1027.
[47] J. H. Holland, *Adaptation in Natural and Artificial Systems* (The University of Michigan Press, Ann Arbor, 1975).
[48] T. Kozek, T. Roska, and L. O. Chua, IEEE Trans. Circuits Syst., I: Fundam. Theory Appl. **40**, 392 (1993).
[49] R. Kunz and R. Tetzlaff, in *Proceedings of the 6th IEEE International Workshop on Cellular Neural Networks and Their Applications*, edited by L. Fortuna (IEEE, Piscataway, NJ, 2000), pp. 241–246.
[50] A. Müller, H. Osterhage, R. Sowa, R. G. Andrzejak, F. Mormann, and K. Lehnertz, J. Neurosci. Methods **152**, 190 (2006).
[51] A. Zarandy, C. Rekeczky, P. Foldesy, and I. Szatmari, J. Circuits Syst. Comput. **12**, 769 (2003).
[52] A. Rodriguez-Vazquez, G. Linan-Cembrano, L. Carranza, E. Roca-Moreno, R. Carmona-Galan, F. Jimenez-Garrido, R. Dominguez-Castro, and S. E. Meana, IEEE Trans. Circuits Syst., I: Fundam. Theory Appl. **51**, 851 (2004).
[53] T. Sauer, J. A. Yorke, and M. Casdagli, J. Stat. Phys. **65**, 579 (1991).
[54] H. D. I. Abarbanel, R. Brown, J. L. Sidorowich, and L. S. Tsimring, Rev. Mod. Phys. **65**, 1331 (1993).
[55] J. P. Egan, *Signal Detection Theory and ROC Analysis* (Academic, New York, 1975).
[56] S. Hallerberg, E. G. Altmann, D. Holstein, and H. Kantz, Phys. Rev. E **75**, 016706 (2007).
[57] M. Laiho, A. Paasio, A. Kananen, and K. Halonen, Int. J. Circuit Theory Appl. **30**, 165 (2002).
[58] M. Laiho, A. Paasio, A. Kananen, and K. Halonen, IEEE Trans. Circuits Syst., I: Fundam. Theory Appl. **51**, 286 (2004).
[59] G. Geis, M. Reinisch, R. Tetzlaff, and F. Puffer, in *Proceedings of the 8th IEEE International Workshop on Cellular Neural Networks and their Applications*, edited by T. Roska, M. Gilli, B. Shi, and A. Zarandy (Amulett'98 Kft., Budapest, 2004), pp. 393–398.
[60] D. Feiden and R. Tetzlaff, Proc. SPIE **5117**, 470 (2003).